Driver-pulse configuration of the nickel-like Ta x-ray laser at 4.48 nm

J. Y. Zhong,[1,2] C. Wang,[1,3] J. Zhang,[1,*] X. Lu,[1] G. Zhao,[2] J. L. Zeng,[2] M. F. Gu,[4] and S. J. Wang[3]
[1]*Laboratory of Optical Physics, Institute of Physics, Chinese Academy of Sciences, Beijing 100080, China*
[2]*National Astronomical Observatories, Chinese Academy of Sciences, Beijing 100012, China*
[3]*National Laboratory on High Power Laser and Physics, Shanghai 201800, China*
[4]*Kavli Institute for Particle Astrophysics and Cosmology, Department of Physics, Stanford University, Stanford, California 94305, USA*
(Received 23 March 2004; revised manuscript received 6 July 2004; published 4 November 2004)

Atomic data (energy levels, radiative rates, electron collision strengths, and excitation rate coefficients) of 107 fine-structure levels of the $(1s^22s^22p^6)3s^23p^63d^{10}$, $3s^23p^63d^94l$, $3s^23p^53d^{10}4l$, and $3s3p^63d^{10}4l$ ($l=s,p,d,f$) configurations of nickel-like Ta ions are calculated using the distorted-wave approximation. Coupled with these atomic data, a hydrodynamic code MED103 is used to optimize the nickel-like Ta x-ray laser at 4.48 nm. Using the optimized drive-pulse configuration, an experiment is conducted to generate the nickel-like Ta x-ray laser at 4.48 nm.

DOI: 10.1103/PhysRevA.70.053803 PACS number(s): 42.55.Vc

I. INTRODUCTION

An important objective in the development of x-ray lasers is to deliver a coherent, saturated output at wavelengths towards the water window [1]. Such saturated x-ray lasers are required for the holography [2] and microscopy [3] of biological specimens and for the deflectometry [4], interferometry [5], and radiography [6] of dense plasmas relevant to inertial confinement fusion and laboratory astrophysics [5]. Nickel-like x-ray lasers, in principle, have a more favorable scaling of laser wavelength with drive-laser energy [7,8]. With the prepulse technique [9–11] and multi target design [12,13], a saturated output has been demonstrated for nickel-like Ag, Sm, and Dy x-ray lasers [7,8,14,15]. It is suggested that the drive energy of nickel-like x-ray lasers can be significantly reduced by further optimizing the drive-pulse configuration [7,8,14–17]. For this purpose, much effort has been made in the research of nickel-like x-ray lasers.

However, few atomic data were published for high-Z nickel-like ions because of their complicated energy structures. Though some high-Z atomic data such as energy levels and radiative rates were reported in the literature, they still have not met with the needs of the rapid development of x-ray lasers. Hagelstein [18] calculated the lowest 107 fine-structure levels of the nickel-like Gd ions, belonging to the $(1s^22s^22p^6)3s^23p^63d^{10}$, $3s^23p^63d^94l$, $3s^23p^53d^{10}4l$, and $3s3p^63d^{10}4l$ ($l=s,p,d,f$) configurations. The radiative rates between the levels were obtained using a relativistic atomic structure code called YODA. Aggarwal *et al.* [19] reported energy levels and radiative rates for dipole-allowed transitions of nickel-like Nd, Sm, Eu, Ta, and W ions using the multi configuration Dirac-Fock method implemented by the GRASP code. They also calculated the electron collision strengths and excitation rates for the Gd XXXVII ions as a test case using the Dirac atomic R-matrix code (DARC) [20].

In this paper, the energy levels and transition probabilities of nickel-like Ta ions are calculated using a flexible atomic code (FAC) developed by one of us [21]. The modified version of a one-dimensional Lagrangian hydrodynamic code MED103 [22] coupled with the calculated atomic data is used to optimize the drive-pulse configuration for the nickel-like Ta x-ray laser at 4.48 nm. Using the optimized drive-pulse configuration, an experiment is conducted. The experimental results confirm the theoretical prediction on the optimized drive-pulse configuration for the performance of the nickel-like Ta x-ray laser at 4.48 nm.

II. ATOMIC DATA

A. Energy levels and radiative rates

The energy levels and transition probabilities for the $(1s^22s^22p^6)3s^23p^63d^{10}$, $3s^23p^63d^94l$, $3s^23p^53d^{10}4l$, and $3s3p^63d^{10}4l$ ($l=s,p,d,f$) configurations of nickel-like Ta ions are calculated using the FAC [21]. It is a fully relativistic approach based on the Dirac equation. The FAC integrates various atomic processes within a unified theoretical framework, ensures the self-consistency between different parts, and provides a uniform, flexible, and user-friendly interface for implementing all computational tasks. Configuration interactions between the configurations mentioned above are included in the present calculations. In Table I we list the main levels including $4p$, $4d$, and $4f$ and we can see our results agree within 1 eV with the GRASP [19] calculations. The other level data are collected from another reference [23]. For some levels with strong mixing there is no good way to identify them and no experimental data exist to clarify them. Therefore some levels might be misplaced for the 107 fine-structure levels. However, we are only interested in the $4d$-$4p$ ($J=0-1$) laser transitions where the order of the related levels is correct.

For the radiative rates we only consider dipole-allowed transitions. Due to the length limitations of this paper, here we cannot list all $E1$ transitions. But when we simulate the nickel-like Ta x-ray laser, all $E1$ transitions are considered. In Table II the oscillator strength and radiative rate are listed for the levels which are connected with the x-ray lasers.

*Electronic address: jzhang@aphy.iphy.ac.cn

TABLE I. Energy levels and state definitions for nickel-like Ta ions and the collision strength with scattered electron energy at 1500 eV from the ground level to the excited levels. $a[\pm b]=a\times10^{\pm b}$.

Index	State configuration	Energy (eV)			Collision strength 1500 eV (from 1 to)
		J^π	FAC	GRASP [19]	
1	$3s^2 3p_{1/2}^2 3p_{3/2}^4 3d_{3/2}^4 3d_{5/2}^6$	0^e	0.00	0.00	0.00
9	$3s^2 3p_{1/2}^2 3p_{3/2}^4 3d_{3/2}^3 3d_{5/2}^6 4p_{1/2}$	1°	1663.49	1662.92	2.7001[−3]
12	$3s^2 3p_{1/2}^2 3p_{3/2}^4 3d_{3/2}^4 3d_{5/2}^5 4p_{3/2}$	1°	1696.78	1696.18	4.1472[−3]
36	$3s^2 3p_{1/2}^2 3p_{3/2}^4 3d_{3/2}^3 3d_{5/2}^6 4d_{3/2}$	0^e	1947.33	1946.33	3.9160[−2]
59	$3s^2 3p_{1/2}^2 3p_{3/2}^4 3d_{3/2}^3 3d_{5/2}^6 4f_{5/2}$	1°	2101.10	2101.67	1.3837[−1]

B. Collision strengths and excitation rate coefficients

In this paper we use the FAC to calculate the impact collision strengths with relativistic distorted-wave approximation. Special attention has been paid to the long-range contributions to the continuum-continuum radial integral by using a phase-amplitude method for the continuum wave functions. To ensure the convergence of the collision strengths, large angular momentum contributions (the maximum partial waves up to 50) have been taken into account. Higher partial-wave contributions have been included using the Coulomb-Bethe approximation [24]. It is vital to ensure convergence in the calculation. We perform the calculations of collision strengths at 20 energies of the scattered electron from 10 to 50 000 eV. These calculations are less time consuming than the close-coupling method like DARC, which is based on solving a set of close-coupling equations. Figure 1 shows, as an example, our calculated collision strength as a function of scattered electron energy for the transition from the ground level to $3s^2 3p_{1/2}^2 3p_{3/2}^4 3d_{3/2}^3 3d_{5/2}^6 4d_{3/2}$ (level No. 36). From the figure one can see that the collision strength is a smooth function of scattered electron energy. It is changed by less than 10% when the scattered electron energy is varied from 100 to 10 000 eV. The effective collision strength can be obtained by integrating the collision strength over a Maxwellian distribution

$$\Upsilon(T_e)_{ij}=\int_0^\infty \Omega(E)_{ij}\exp\left(-\frac{E}{kT_e}\right)d\left(\frac{E}{kT_e}\right), \tag{1}$$

where E is the scattered electron energy, k is Boltzmann's constant, and T_e is the electron temperature in K. Obviously, the effective collision strength is a function of the temperature. In practical applications, one usually needs the excitation rate coefficients ($\mathrm{cm^3\ s^{-1}}$) in the statistical equilibrium to obtain the populations. It can be obtained from the effective collision strength

$$C_1(T_e)_{ij}=\frac{8.629\times10^{-6}}{g_i\sqrt{kT_e}}e^{-E_{ij}/kT_e}\Upsilon(T_e)_{ij}, \tag{2}$$

where E_{ij} is the energy difference between levels i and j, and g_i is the statistical weight of level i. The deexcitation rates are obtained by detailed balancing. In Fig. 2 we show the rate coefficient as a function of temperature for the same transition 1-36 as in Fig. 1. For comparison, the result obtained by Daido *et al.* [25] has also been given in Fig. 2. Daido *et al.* obtain the rate coefficient from a fitting formula

$$C_2(T_e)(i\to j)=1.58\times10^{-5}\frac{np(b)\exp(-b)}{\Delta E_{i\to j}\sqrt{kT_e}}, \tag{3}$$

where the notation $p(b)$ is described as

$$\ln p(b)=A_0+A_1\ln b+A_2(\ln b)^2+A_3(\ln b)^3, \tag{4}$$

where b is $\Delta E_{ij}/kT_e$, n the multiplier, and A_i ($i=0,1,2,3$) the fitting parameters. These fitting formula results represent the results of the YODA code [25].

Practical calculations show that the effective collision strength at a given temperature is very close to the collision strength of the scattered electron energy which has the same value as the temperature. For example, the effective collision strength for 1-36 is 0.039 16 at a temperature of 1500 eV. At a scattered electron energy of 1500 eV, the collision strength for this transition is 0.039 40, which is very close to the value 0.039 16. The desired electron temperature is 1–1.5 keV for the nickel-like Yb ($Z=70$) x-ray laser and 1.4–1.8 keV for the nickel-like W ($Z=74$) x-ray laser [25].

TABLE II. Oscillator strength and radiative rate for allowed transitions in the nickel-like Ta ion. $a[\pm b]=a\times10^{\pm b}$.

Transition $j\to i$	f_{ij}	A_{ji} ($\mathrm{s^{-1}}$)	A_{ji} ($\mathrm{s^{-1}}$) [19]
9→1	1.4018[−1]	5.6158[+12]	5.9385[+12]
12→1	2.5877[−1]	1.0786[+13]	1.1522[+13]
59→1	5.9346[+0]	3.7907[+14]	4.0104[+14]
36→9	2.4321[−1]	8.4963[+11]	8.2451[+11]
36→12	1.7249[−1]	4.6934[+11]	4.3657[+11]
59→36	2.5424[−1]	8.6622[+10]	7.8153[+10]

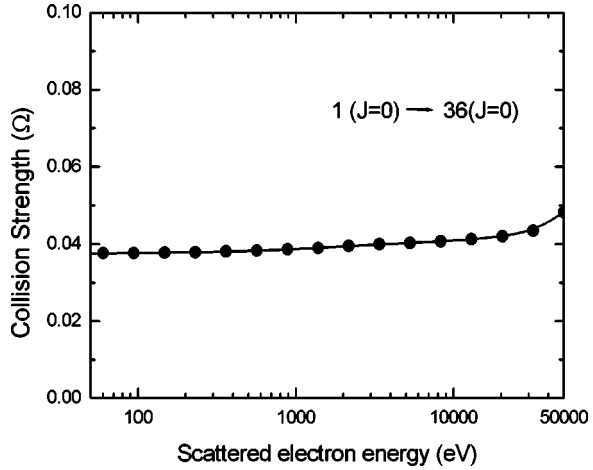

FIG. 1. Collision strengths for the transition from the ground level $[3s^2 3p^6 3d^{10}\ (J=0)]$ to the upper laser level $[3s^2 3p^6 3d^9 4d\ (J=0)]$ (1-36) of Ni-like Ta ions.

For the nickel-like Ta ($Z=73$) x-ray laser we assume it to be 1500 eV. Therefore in the MED103 code, the effective collision strength is approximated by the collision strength at a scattered electron energy of 1500 eV. Thus the excitation rate coefficient is obtained by

$$C_3(T_e)_{ij} = \frac{8.629 \times 10^{-6}}{g_i \sqrt{kT_e}} e^{-E_{ij}/kT_e} \Omega(1500\ \mathrm{eV})_{ij}. \qquad (5)$$

The excitation rate coefficients obtained from Eq. (5) are also shown in Fig. 2. It can be seen that the rate coefficients obtained by Eq. (5) agree well with the two results mentioned above. In Table I we have also listed the collision strengths from the ground level to the other excited levels which are connected with the x-ray lasers at a scattered electron energy of 1500 eV.

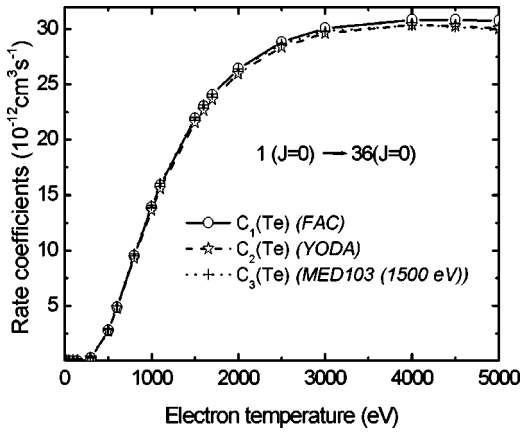

FIG. 2. Collisional excitation rates as a function of electron temperature for the transition from the ground level $[3s^2 3p^6 3d^{10}\ (J=0)]$ to the upper laser level $[3s^2 3p^6 3d^9 4d\ (J=0)]$ in Ni-like Ta ions. The solid line with circle is calculated by FAC and the dashed line with star is from the YODA code; the dotted line with plus is the rate used in the MED103 code.

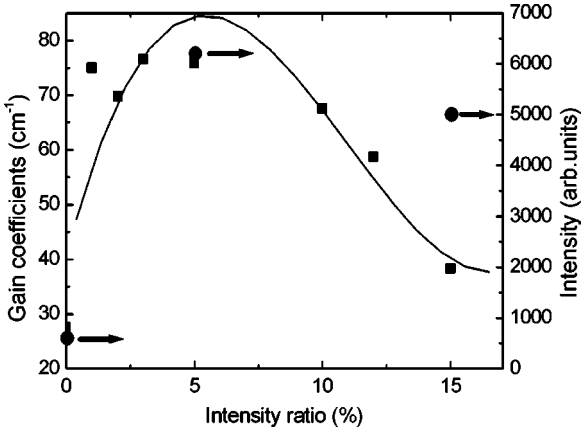

FIG. 3. By changing the intensity of the prepulse to the main pulse with their delay time fixed as 1.5 ns, we get different gain coefficients. The figure shows that a better performance could be obtained at ratio of 1–10 %. The rectangle dot and the fitting curve are our simulation results and the circular dot with right arrow is the experimental results.

III. SIMULATIONS OF THE NICKEL-LIKE Ta X-RAY LASER

Based on the atomic data, we perform simulations to optimize the performance of the nickel-like Ta x-ray laser at 4.48 nm. The modified version of the one-dimensional Lagrangian hydrodynamic code MED103 [22] coupled with the results of FAC is used to simulate the time evolution of laser-plasma interactions and gain coefficients. In the simulation, we intend to find out the optimized parameters by changing the intensity ratio between the prepulse and the main pulse and the separation time between the prepulse and main pulse. The durations of the prepulse and main pulse are both 100 ps. The intensity of the main pulse is fixed as 3×10^{14} W cm^{-2}. Figure 3 shows the dependence of the gain coefficient on the ratio between the prepulse and the main pulse intensity when their delay time is fixed as 1.5 ns. We find that the optimum ratio of the prepulse to the main pulse is 2%–10%. This driver-pulse configuration can produce a peak gain coefficient with a value of 70 cm^{-1}.

Figure 4 shows peak gain coefficients for different separation times between the prepulse and the main pulse when the intensity of the prepulse is fixed as 1.5×10^{13} W cm^{-2}. We find that the optimum delay time is 1.5–1.6 ns. Figure 5(A) shows the nickel-like Ta ion fraction versus space and time in the plasma generated by the optimized drive-pulse configuration, in which the separation between the prepulse and the main pulse is 1.5 ns and the intensity ratio is 5%. The peak intensity of the main pulse is 3×10^{14} W cm^{-2}, which occurs at 1.62 ns. In Fig. 5(B) the contour of the nickel-like Ta x-ray laser gain at 4.48 nm is shown by the same driver-pulse configuration. The gain coefficient can be more than 50 cm^{-1}.

IV. EXPERIMENTS

The experiments were performed on the Shenguang II laser facility in Shanghai. The double-target coupling tech-

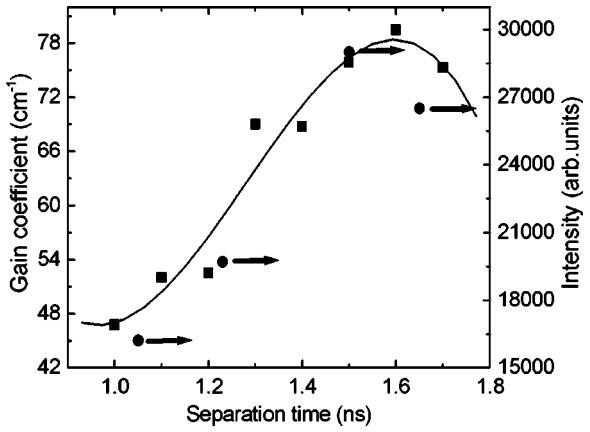

FIG. 4. By changing the separation time between the prepulse and the main pulse with the intensity of the prepulse fixed as 1.5×10^{13} W cm^{-2}, we get different gain coefficients. The figure showed that the good gain coefficient could be obtained at 1.5–1.6 ns duration time. The rectangle dot and the fitting curve are our simulation results and the circular dot with right arrow is the experimental results.

nique and mixed-wavelength pumping scheme were used in the experiments. The two pumping beams of the Shenguang II laser at fundamental and double-frequency wavelengths ($\lambda_1 = 1.053$ μm, $\lambda_2 = 0.53$ μm) with a 100-ps duration were used in a five-element cylindrical lens array (CLA) line focus system, which provides a line focus with a 6-mm length and a 100-μm width, giving an irradiance of 2.5×10^{14} W cm^{-2}. They irradiate the target with a 42° incidence angle as shown in Fig. 6(A). Deploying the other two mixed-wavelength beams in 180° opposed in a second line focus produced a plasma with an opposed density gradient that compensates for refractive deviation of the x-ray laser beam from the first plasma. The flat slab targets were 5-mm-long, 4-mm-width, 1-μm-thick Ta stripes coated on glass substrates. Both ends of the slab target were placed well within the line focus to avoid cold plasmas at the ends of the targets. The targets

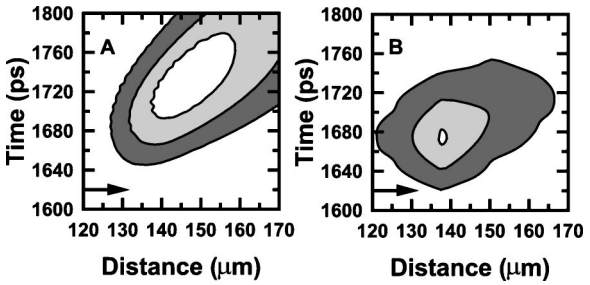

FIG. 5. (A) The nickel-like Ta ion fraction vs space and time in the plasma generated by 100-ps double pulse irradiance with a peak intensity of 3×10^{14} W cm^{-2}. The right arrow on the 1620 ps is the time when the peak of optical laser occurs. The fraction in plot is from 60% (white) to 20% (gray) by a step of 20%. (B) Contours of nickel-like Ta x-ray laser gain at 4.48 nm generated by 100-ps double-pulse configuration at 3×10^{14} W cm^{-2} peak irradiance. The energy of the prepulse was set 5% of the main pulse and delayed time was 1.5 ns. The gain is plotted from 50 cm^{-1} (white) to 10 cm^{-1} (gray) by a step of 20 cm^{-1}.

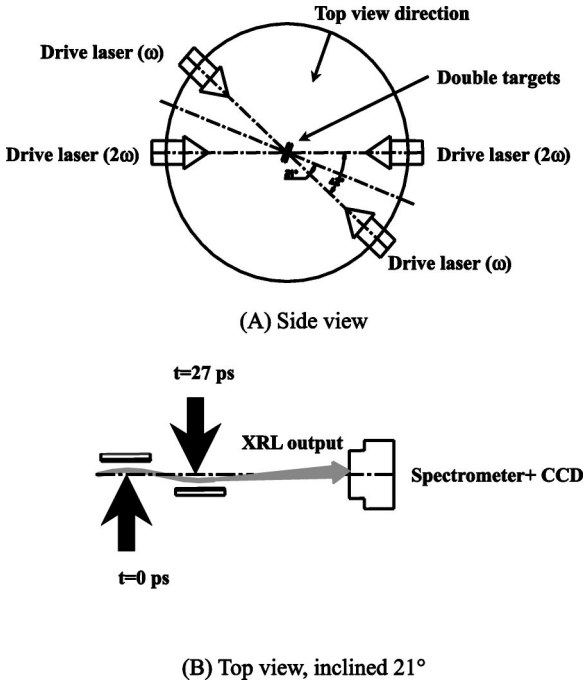

FIG. 6. (A) Side view of experimental setup of the Ni-like Ta x-ray laser. Two different frequency laser beams irradiate the targets with a 42° incidence angle. (B) Top view of experimental setup. The drive beams for the first slab target arrive 27 ps earlier than the beams for the second target.

were aligned so that they were parallel with an adjustable separation (in the direction perpendicular to the target surfaces) between the surface planes and an axial separation of 3 mm between the two targets. Because the duration of the x-ray laser pulse is comparable to the propagation time, it is necessary to achieve a traveling-wave excitation for the two successive targets to maximize the amplification. To approximate this condition, as shown in Fig. 6(B) we timed the drive beams for the first slab target to arrive 27 ps earlier than the beams for the second target. The primary diagnostics along the target axis was a flat-field grazing incidence x-ray spectrometer with aperiodically ruled gratings of 2400 lines per millimeter. The x-ray laser spectrum was recorded on an x-ray charge-coupled-device (CCD) detector. In our experiments each laser beam was divided into a prepulse and a main pulse by a pulse splitting system in the beam path. The ratio of the prepulse to the main pulse was about 4% and the main pulse was delayed about 1.0–1.7 ns to the prepulse. The separation between two targets surfaces was adjusted from 50 μm to 100 μm in order to find an optimal separation and obtain a maximum x-ray laser output.

Figure 7 shows a typical spectrum of the nickel-like x-ray laser at 4.48 nm. This result is obtained for two coupled 5-mm-long targets with an optimized lateral separation of 50 μm. There was a C_8H_8 filter to attenuate the intensity by a factor of 1.2 for 4.5 nm in front of the CCD detector, bringing the clear absorbing edge of carbon at 4.37 nm. Based on the edge, the wavelength of laser line was accurately determined to be 4.48 nm. The laser line intensity at 4.48 nm was measured for different drive-pulse configurations. In order to compare the experimental result with the

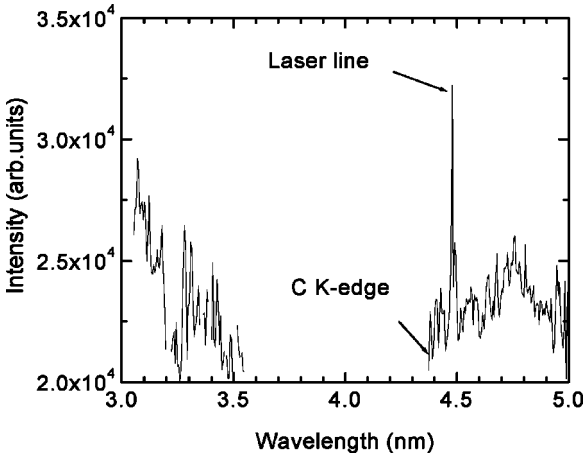

FIG. 7. A typical spectrum of the nickel-like Ta x-ray laser, where the laser line at 4.48 nm stands up, The absorption edge of C can be seen at 4.37 nm.

simulation, the measured laser intensity versus the ratio of the prepulse to the main pulse is plotted in the same figure with the simulation results (circular dots with the right arrow in Fig. 3), from which a similar tendency is found. The dependence of the measured laser intensity versus the separation time between the prepulse and the main pulse is also compared in Fig. 4. Both experimental and simulation give an optimized separation time of 1.5 ns. In order to determine an effective gain coefficient, the dependence on the plasma length was investigated. The data and the fitting curve with the Linford formula are shown in Fig. 8 and the efficient gain-length product is 5.5.

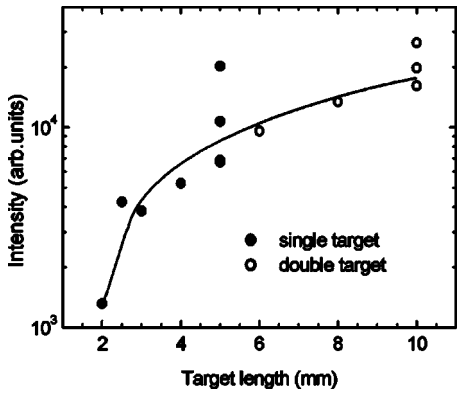

FIG. 8. The output intensity of the nickel-like Ta x-ray laser as a function of the plasma length. The total gain-length product is about 5.5.

V. CONCLUSION

In conclusion, we have numerically optimized the drive-pulse configuration for the performance of the nickel-like Ta x-ray laser at 4.48 nm using the one-dimensional hydrodynamic code MED103 coupled with the FAC atomic code. An experiment is carried out using four laser beams at fundamental and double-frequency wavelengths, respectively, from the SHENGUNG II laser facility. The experiment confirms the optimized drive-pulse configuration.

ACKNOWLEDGMENTS

This work is jointly supported by the NSFC under Grant Nos. 10176034, 10433010, and 10374114 and the NKBRSF under Grant Nos. G1999075206 and G1999075406 and the National Hi-tech ICF program.

[1] R. C. Elton, *X-Ray Lasers* (Academic Press, New York, 1990).
[2] J. E. Trebes, S. B. Brown, E. M. Campbell, D. L. Matthews, D. G. Nilson, G. F. Stone, and D. A. Whelan, Science **238**, 517 (1987).
[3] L. B. Da Silva, J. E. Trebes, R. Balhorn, S. Mrowka, E. Anderson, D. T. Attwood, T. W. Barbee, J. Brase, M. Corzett, J. Gray, J. A. Koch, C. Lee, D. Kern, R. A. London, B. J. MacGowan, D. L. Matthews, and G. Stone, Science **258**, 269 (1992).
[4] D. Ress, L. B. Da Silva, R. A. London, J. E. Trebes, S. Mrowka, R. J. Procassini, T. W. Barbee, Jr., and D. E. Lehr, Science **265**, 514 (1994).
[5] R. Cauble, L. B. Da Silva, T. W. Barbee Jr., P. Celliers, C. Decker, R. A. London, J. C. Moreno, J. E. Trebes, A. S. Wan, and F. Weberet, Science **273**, 1093 (1996).
[6] D. H. Kalantar, M. H. Key, L. B. DaSilva, S. G. Glendinning, J. P. Knauer, B. A. Remington, F. Weber, and S. V. Weber, Phys. Rev. Lett. **76**, 3574 (1996).
[7] J. Zhang, A. G. MacPhee, J. Nilsen, J. Lin, T. W. Barbee Jr., C. Danson, M. H. Key, C. L. S. Lewis, D. Neely, R. M. N. O'Rourke, G. J. Pert, R. Smith, G. J. Tallents, J. S. Wark, and E. Wolfrum, Phys. Rev. Lett. **78**, 3856 (1997).
[8] J. Zhang, A. G. MacPhee, J. Lin, E. Wolfrum, R. Smith, C. Danson, M. H. Key, C. L. S. Lewis, D. Neely, J. Nilsen, G. J. Pert, G. J. Tallents, and J. S. Wark, Science **276**, 1097 (1997).
[9] J. Nilsen, B. J. MacGowan, L. B. Da Silva, and J. C. Moreno, Phys. Rev. A **48**, 4682 (1993).
[10] J. Nilsen and J. C. Moreno, Phys. Rev. Lett. **74**, 3376 (1995).
[11] J. Nilsen and J. C. Moreno, Opt. Lett. **20**, 1386 (1995).
[12] A. Carillon, H. Z. Chen, P. Dhez, L. Dwivedi, J. Jacoby, P. Jaegle, G. Jamelot, Jie Zhang, M. H. Key, A. Kidd, A. Klisnick, R. Kodama, J. Krishnan, C. L. S. Lewis, D. Neely, P. Norreys, D. O'Neill, G. J. Pert, S. A. Ramsden, J. P. Raucourt, G. J. Tallents, and J. Uhomoibhi, Phys. Rev. Lett. **68**, 2917 (1992).
[13] S. J. Wang, Y. Gu, G. L. Zhou, Y. L. Ni, S. Y. Yu, S. Z. Fu, C. S. Mao, Z. C. Tao, W. N. Chen, Z. Q. Lin, D. Y. Fan, G. P. Zhang, J. T. Sheng, M. L. Yang, T. X. Zhang, Y. F. Shao, H. M. Peng, X. T. He, and M. Yu, Chin. Phys. Lett. **8**, 618 (1991).
[14] J. Y. Lin, G. J. Tallents, J. Zhang, A. G. MacPhee, C. L. S. Lewis, D. Neely, J. Nilsen, G. J. Pert, R. M. N. O'Rourke, R. Smith, and E. Wolfrum, Opt. Commun. **158**, 55 (1998).
[15] R. Smith, G. J. Tallents, J. Zhang, G. J. Pert, and E. Wolfrum, Phys. Rev. A **59**, R47 (1999).
[16] T. Ozaki, R. A. Ganeev, A. Ishizawa, T. Kanai, and H. Kuroda, Phys. Rev. Lett. **89**, 253902 (2002).

[17] X. Lu, J. Y. Zhong, Y. J. Li, and J. Zhang, Phys. Plasmas **10**, 2978 (2003).
[18] P. L. Hagelstein, Phys. Rev. A **34**, 874 (1986).
[19] K. M. Aggarwal, P. H. Norrington, K. L. Bell, F. P. Keenan, G. J. Pert, and S. J. Rose, At. Data Nucl. Data Tables **74**, 157 (2000).
[20] P. H. Norrington and I. P. Grant (unpublished).
[21] M. F. Gu, Astrophys. J. **582**, 1241 (2003).
[22] J. P. Christiansen, D. E. T. F. Ashby, and K. V. Roberts, Comput. Phys. Commun. **7**, 271 (1974).
[23] J. Y. Zhong, J. L. Zeng, J. Zhang, G. Zhao, and M. F. Gu, At. Data Nucl. Data Tables (to be published).
[24] A. Burgess and V. B. Sheorey, J. Phys. B **7**, 2403 (1974).
[25] H. Daido, S. Ninomiya, T. Imani, Y. Okaichi, M. Takagi, R. Kodama, H. Takabe, Y. Kato, F. Koike, J. Nilsen, and K. Murai, Int. J. Mod. Phys. B **11**, 945 (1997).